

# Pharmacophore Modeling and Docking Study of Pyrazolylaminoquinazoline Derivatives as Highly Potent Fibroblast Growth Factor Receptor Inhibitors<sup>2</sup> (FGFR2)

LUMINITA CRISAN, DANIELA VARGA, LILIANA PACUREANU\*

Institute of Chemistry Timisoara of Romanian Academy, Department of Computational Chemistry, 24 Mihai Viteazul Blvd., 300223, Timisoara, Romania

*In this study pharmacophore modeling and molecular docking investigations have been performed on pyrazolylaminoquinazoline derivatives, highly potent fibroblast growth factor receptor<sup>2</sup> (FGFR2) inhibitors. The best pharmacophore hypotheses displaying five features (ADHRR.2051 and AADHR.798) were generated using a set of 28 compounds. The associated 3D atom-based quantitative structure – activity relationships (QSAR) models were statistically robust showing high correlation coefficients ( $R$ -squared = 0.981 / 0.982), and cross validation coefficients ( $Q$ -squared = 0.645 / 0.671). The  $R$ -Pearson values for the test set of 0.805 / 0.820 indicate that the models are robust and exhibit good predictive power. The interactions of pyrazolylaminoquinazoline with FGFR2 binding site revealed two hydrogen bonds with Ala567. The obtained pharmacophore, 3D atom-based QSAR models and binding features resulted from docking studies can help medicinal chemists to design new pyrazolylaminoquinazoline inhibitors with improved potency.*

**Keywords:** Pharmacophore modeling, QSAR, docking, pyrazolylaminoquinazoline

Fibroblast growth factor receptors (FGFRs) are included into receptor tyrosine kinase (RTK) family [1] and are currently targeted for novel oncologic therapies. FGFRs are involved in several critical biological processes including morphogenesis, differentiation, patterning, and cell migration [2]. They network with multiple fibroblast growth factors (FGFs), to stimulate development [2]. The FGFR2 gene is confined on the chromosome 10q26.13 displaying about 21 exons which by alternative splicing spawn multiple protein isoforms [3]. FGFR isoforms include seven receptors, as follows: FGFR1b, FGFR1c, FGFR2b, FGFR2c, FGFR3b, FGFR3c and FGFR4 [4]. The kinase domain of FGFR2 is situated in the area delimited by the residues 458–768.

Today's computational chemistry is widely involved in early stages of drug discovery programs. Ligand- and structure-based virtual screening is efficient approaches which can reduce large chemical libraries of compounds to a smaller list of potentially active molecules [5, 6]. Pharmacophore modeling is one of the successful tool in computer-aided drug discovery and development which can be applied in various stages i.e., virtual screening, lead optimization, *de novo* design, side effect / off-target prediction and target identification. Pharmacophore modeling identifies the key elements of molecular recognition and help to correlate the observed biological activities of chemical compounds with their chemical structures. Pharmacophore models are useful tools to mine chemical databases to identify new chemical entities with various scaffolds (the so called *scaffold-hopping potential*) [6-9]. In drug design quantitative structure–activity relationships (QSAR) is a concept which can contribute markedly to accurate prediction of biological activities. QSAR rely on the hypothesis that fluctuation of the biological activity of the compounds is associated with differences in their structural characteristics [7]. Besides biological activity prediction, another aim of QSAR analysis is to direct ligand-based design of new analogue series [8, 10]. Molecular docking allows to explore the interaction pattern of a small molecule with a biological target and to confirm

the conclusions of pharmacophore and QSAR investigations [11-13]. Current interest in drug design is related to pharmacophore models which are linked to molecular docking to consensually improve virtual screening results [11, 12].

To the best of our knowledge, the series of 28 pyrazolylaminoquinazoline derivatives [14] - highly potent FGFR2 inhibitors have not been investigated computationally [14]. Therefore, the current work aims at using relevant structural information from these ligands to develop pharmacophore models. The pharmacophore models will be validated by 3D atom-based QSAR and docking to provide an extensive picture of pyrazolylaminoquinazoline interaction with FGFR2.

## Experimental part

### Dataset

A dataset comprising 28 pyrazolylaminoquinazoline derivatives potent fibroblast growth factor receptor inhibitors, FGFR2 (table 1) were collected from a recent publication [14] and used in the current study. The molecular structures of all 28 pyrazolylaminoquinazoline derivatives were sketched with the help of Symyx Draw software [15] and saved as smiles codes.

### Pharmacophore 3D-QSAR modeling

Phase module [16-18] of Schrodinger 2016-1 suite [19] was used to develop the pharmacophore hypotheses and their corresponding 3D-QSAR models for 28 pyrazolylaminoquinazoline derivatives. The structures were prepared using the standard protocol including generation of ionization states and tautomers at physiological pH (7.4±0.2), remove salts [20], conformational expansion and energy minimization based on the OPLS-2005 force field [21, 22]. The experimental biological activities,  $IC_{50}$ , were transformed into negative logarithm of inhibitory concentrations,  $pIC_{50}$ . In the pharmacophore generation step the threshold for active compounds was set to  $pIC_{50} > 9.3$  (8 compounds in picomolar range), for inactives was

\* email: pacureanu@acad-icht.tm.edu.ro

**Table 1**  
 THE STRUCTURES OF PYRAZOLYLAMINOQUINAZOLINE DERIVATIVES, THEIR EXPERIMENTAL ( $pIC_{50_{EXP}}$ ) AND PREDICTED ( $pIC_{50_{PRED}}$ ) ACTIVITY VALUES OBTAINED BY 3D ATOM BASED QSAR

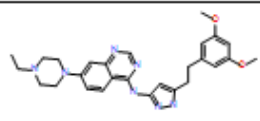
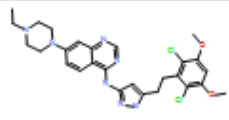
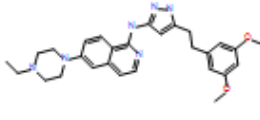
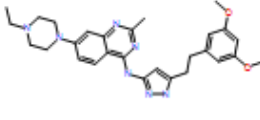
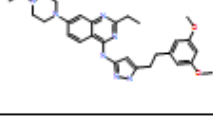
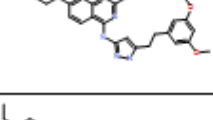
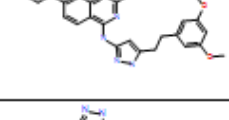
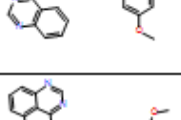
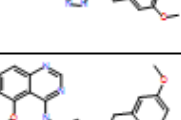
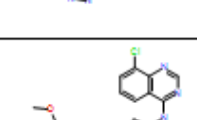
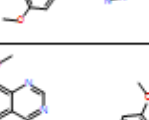
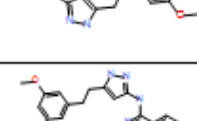
No*	Structure	$pIC_{50_{exp}}$	$pIC_{50_{pred}^S}$	$pIC_{50_{pred}^{2c}}$
1*		9.097	9.350	9.350
2		9.523	9.410	9.430
3		8.921	8.890	8.860
4*		9.222	9.240	9.270
5		9.301	9.420	9.400
6		9.155	9.120	9.130
7		9.222	9.400	9.360
8		8.495	8.460	8.480
9		7.772	7.820	7.890
10		6.996	6.990	6.910
11*		8.319	8.440	8.470
12		8.409	8.400	8.420
13		8.367	8.350	8.390

Table 1 - CONTINUED

14*		9.000	9.050	9.110
15		9.222	9.300	9.290
16*		9.222	9.220	9.210
17		9.155	9.320	9.310
18		9.046	8.960	8.960
19		8.569	8.670	8.670
20		9.699	9.660	9.230
21*		9.699	9.230	9.260
22*		9.155	9.270	9.270
23		9.046	9.010	9.040
24		9.523	9.450	9.440
25		9.398	9.330	9.320
26*		9.097	8.860	8.900

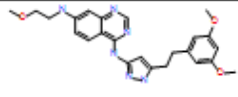
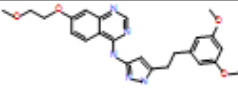
27		9.398	9.250	9.260
28*		8.886	8.870	8.850

Table 1 - CONTINUED

\* compounds designated for the test set;  $pIC_{50_{pred}}^s$  by ADHRR.2051 hypothesis;  $pIC_{50_{pred}}^{ac}$  by AADHR.798 hypothesis

$pIC_{50} < 8.5$  (6 compounds) while the rest of the inhibitors were considered as moderately active. Redundant conformations were removed if heavy atoms root mean squared deviation (RMSD) is greater than 2 Å. Phase recognizes the following built-in pharmacophore features: acceptor (A), donor (D), hydrophobic (H) and ring R (R). In the first step Phase detect the shared set of pharmacophore features relying consistently in actives which display common spatial arrangements. The ranking of pharmacophore hypotheses in order to select the best alignment of the active compounds was carried out using a threshold RMSD of 1.2 Å.

3D atom-based QSAR, consider a molecule as consisting of overlapping van der Waals spheres displaying the following properties: hydrogen-bond donor (D), electron withdrawing (i.e. including hydrogen bond acceptors, W), hydrophobic (H), negative ionic (N), positive ionic (P), and miscellaneous (X) [18]. In order to build the 3D atom-based QSAR model, the data set was randomly split into training set (67%) and test set (33%) used for validation purposes. The atom-based 3D-QSAR model have been developed at three PLS factors in order to avoid overfitting. Automatically, Phase build atom-based 3D QSAR models for all pharmacophore hypotheses developed. Internal and external validation parameters for atom-based 3D QSAR were: squared correlation coefficient R-squared (training set), squared correlation coefficient Q-squared (test set), standard deviation (SD), Pearson's correlation coefficient R-Pearson (test set), RMSE - the root-mean-square error in the test set predictions, statistical significance (P), and Fisher test (F) [20].

### Molecular docking

All ligands were prepared for docking by generation of ionization states and tautomers with LigPrep software, followed by conformational expansion using OMEGA module [23-27] from OpenEye package, retaining a maximum of 200 conformers per compound, an energy cut-off of 10 kcal/mol and RMSD less than 0.8 Å. The 3D structure of FGFR2 kinase domain was extracted from the co-crystal 1OEC deposited in PDB [28] and prepared for docking with Fred Receptor [29] module version 2.2.5 from OpenEye package. The active site box was set to 6933 Å<sup>3</sup>, inner contour of 534 Å<sup>3</sup> and outer contour of 2341 Å<sup>3</sup>, whereas crystallographic water molecules were deleted. The docking procedure was carried out using Fast Rigid Exhaustive Docking (FRED) [30-32] version 3.0, to perform a rigid receptor-flexible ligand docking of pyrazolyl-aminoquinazoline derivatives.

### Results and discussions

#### Pharmacophore modeling

On the basis of performance various pharmacophore models generated were ranked as function of significant statistical parameters R-squared, SD, F, P, RMSE, Q-squared, and Pearson-R. According to the above criteria the best pharmacophore models were selected. A number of ninety-two pharmacophore hypotheses from the total one thousand-six variant hypotheses generated have an R-Pearson > 0.8 and Q-squared > 0.6. Two pharmacophore hypotheses were selected based on statistical parameter values and survival-inactives score. The best QSAR models resulted are based on the alignments provided by pharmacophore hypotheses ADHRR.2051 and AADHR.798: R-squared of 0.981 and 0.982, Q-squared values of 0.645 and 0.641, RMSE values of 0.204 and 0.196, R-Pearson of 0.805 and 0.820, indicating that the models are robust and have good predictive power.

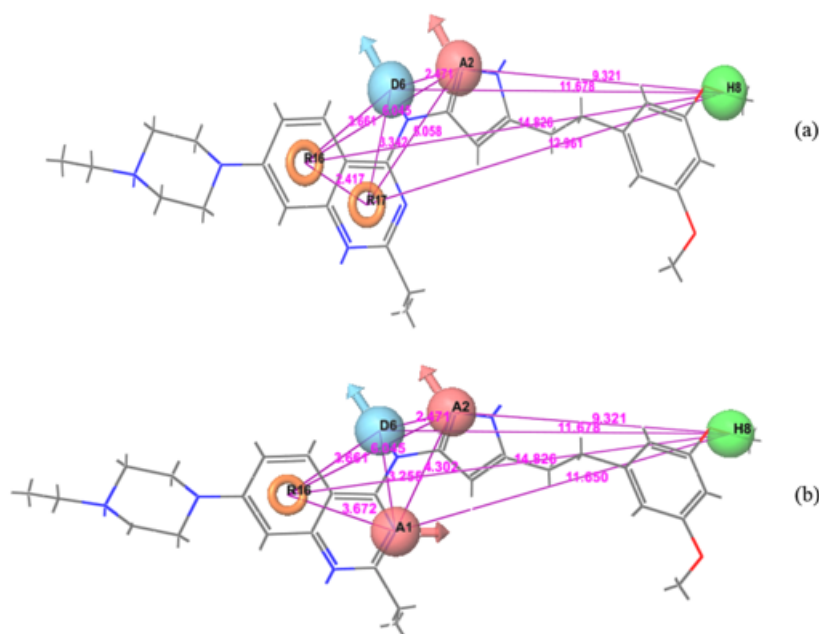


Fig. 1. The pharmacophore hypotheses (a) ADHRR.2051 (acceptor (A2, pink), donor (D6, blue), hydrophobic (H8, green) and ring (R16, orange)); (b) AADHR.798 (acceptor (A1, A2, pink), donor (D6, blue), hydrophobic (H8, green) and ring (R16, orange)) aligned to the compound 5 (best fitness score = 3)

ID	Survival score	Survival-inactive score	Site	Vector	Volume	Selectivity	Energy	Activity	Inactive
ADHRR.2051	3.647	1.933	0.91	0.993	0.747	1.693	0.735	9.301	1.714
AADHR.798	3.623	1.923	0.89	0.995	0.742	1.592	0.735	9.301	1.7
AADRR.1836	3.652	1.893	0.93	0.977	0.745	1.606	0.735	9.301	1.759
AAADR.339	3.628	1.866	0.92	0.977	0.736	1.398	0.735	9.301	1.763
AADRR.1837	3.637	1.822	0.93	0.977	0.727	1.606	1.444	9.699	1.815

**Table 2**  
THE BEST FIVE MODELS DISPLAYING THE HIGHEST SURVIVAL SCORE AND MATCHING ALL ACTIVE COMPOUNDS

Survival score - a weighted sum of site, vector, volume, and a term for the number of matches; survival - inactive - the difference in survival score between actives and inactives; site score - accounts for the proximity of site points in the ligands contributing to the hypothesis, based on the RMS deviation; vector alignment score - record the vectorial fitness for acceptors, donors, and aromatic rings; volume - measures the overlapping volumes of the contributing structures; selectivity - accounts of the infrequency of the hypothesis, according to World Drug Index; energy - the energy difference (kcal/mol) between the reference structure and the lowest energy structure; activity - activity of the reference ligand; inactive - the survival score of inactives.

### Atom-based 3D QSAR

Scatter plots of the experimental *versus* predicted activities of pyrazolylaminoquinazoline derivatives, obtained for ADHRR.2051 and AADHR.798 at 3 PLS factors show good correlative properties and low difference between experimental and predicted values, and are presented in figure 2.

On the basis of the maximal fitness score, the compound **5** (fitness score = 3) was selected as reference compound to perform further studies. In order to investigate the correlation of the most important interactions with biological activity the hydrogen bond donor, hydrophobic, electron withdrawing groups and positive ionic fields were generated for compound **5**. In figures 3-6 the most favorable features are depicted in blue, whereas the detrimental features are indicated in red. We can observe several favorable donor fields localized on NH group,

pyrazole and piperazine rings and one unfavorable hydrogen bond donor area on pyrimidine ring substituent (fig. 3). Large favorable hydrophobic areas extended on the whole molecule accompanied by several unfavorable regions in the central part of the molecule and on H8 can be noticed (fig. 4). Electron withdrawing favorable zones covers piperazine, pyrazole and phenyl ring substituents, but H8 and pyrimidine are partially covered by unfavorable areas (fig. 5). A favorable positive ionic area is located on piperazine ring, whereas an unfavorable zone is observed on pyrimidine ring (fig. 6). Hydrogen bond donor and electron withdrawing fields suggests two favorable areas on NH and pyridazole ring which are susceptible to interact with the receptor.

### Docking

The compound **5** showing the highest affinity towards FGFR2 was chosen to validate by rigid receptor - flexible ligand docking the results obtained by pharmacophore modeling and 3D atom-based QSAR. The acceptor =N- and donor NH<sub>2</sub> groups interact effectively with FGFR-2 binding site by making two hydrogen bonds with Ala567 (PDB ID: 1OEC) at 2.787 Å and at 3.194 Å [33, 34] (see fig.7), similar to compound **7** docked into FGFR1 [14]. This was also suggested by pharmacophore hypotheses ADHRR.2051 and AADHR.798 where =N- corresponds to acceptor site A2 and NH<sub>2</sub> coincide with donor site D6. Hydrogen bond donor and electron withdrawing fields indicated D6 and A2 as favorable areas. The spatial arrangement of acceptor and donor sites inside ADHRR.2051 and ADHRR.798 hypotheses is supported also by the interactions observed into co-crystal structure of

ID	PLS#	SD	R-squared	F	P	RMSE	Q-squared	Pearson-R
ADHRR.2051	1	0.288	0.827	81.100	7.02E-08	0.196	0.671	0.828
	2	0.190	0.929	105.100	6.27E-10	0.223	0.576	0.776
	3	0.100	0.982	266.600	3.13E-13	0.204	0.645	0.805
AADHR.798	1	0.282	0.835	85.800	4.70E-08	0.199	0.662	0.816
	2	0.173	0.942	128.800	1.37E-10	0.218	0.592	0.781
	3	0.098	0.982	276.800	2.37E-13	0.196	0.671	0.820

**Table 3**  
THE STATISTICAL PARAMETERS OF THE ATOM-BASED 3D QSAR MODELS

# Number of PLS factors; SD - standard deviation of the regression; R-squared - the coefficient of determination; F - the ratio of the model variance to the observed activity variance; P - the significance level of variance ratio; RMSE - the root-mean-squared error for the test set predictions; Q-squared - analogous to R-squared based on the test set predictions; Pearson-R - the value for the correlation between the predicted and observed activity for the test set [16-18]

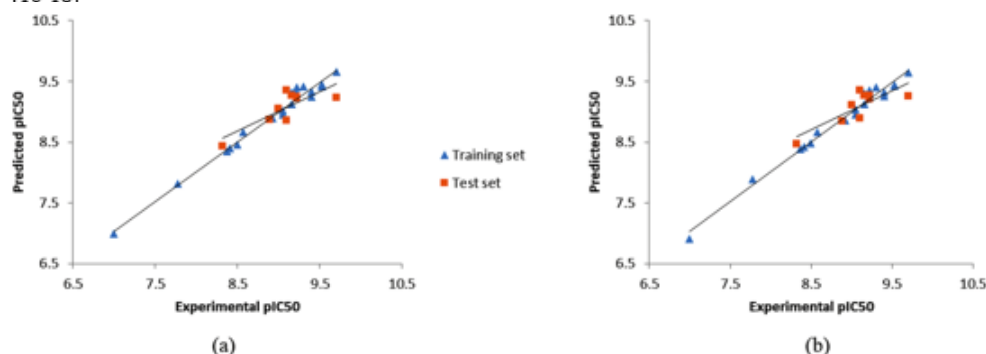


Fig. 2. Experimental *versus* predicted activities for 3D-QSAR models (a) ADHRR2051 and (b) ADHRR798

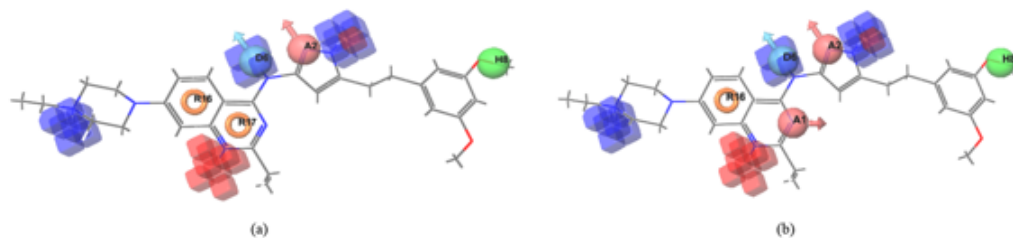


Fig. 3. Favorable (blue) and unfavorable (red) hydrogen bond donor fields for compound 5: (a) ADHRR.2051 and (b) ADHRR.798.

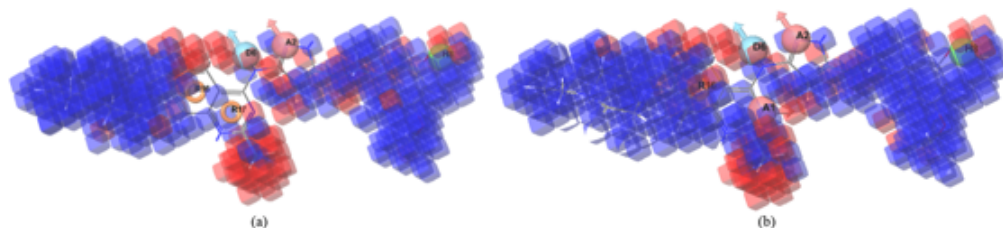


Fig. 4. Favorable (blue) and unfavorable (red) hydrophobic fields for compound 5: (a) ADHRR.2051 and (b) ADHRR.798.

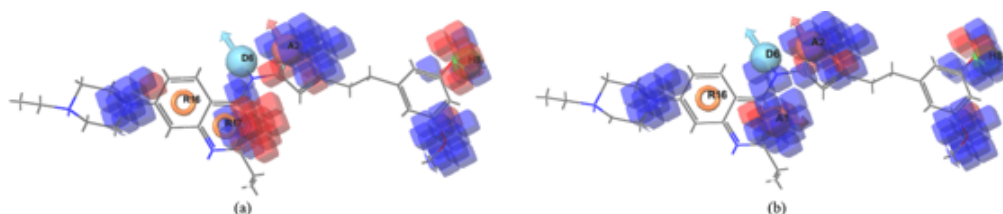


Fig. 5. Favorable (blue) and unfavorable (red) electron withdrawing fields for compound 5: (a) ADHRR.2051 and (b) ADHRR.798.

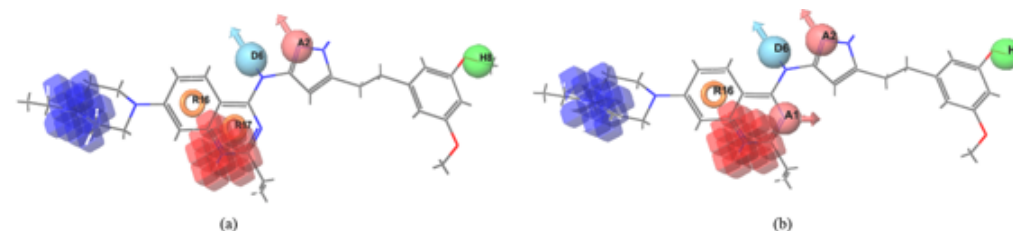


Fig. 6. Favorable (blue) and unfavorable (red) positive ionic fields for compound 5: (a) ADHRR.2051 and (b) ADHRR.798.

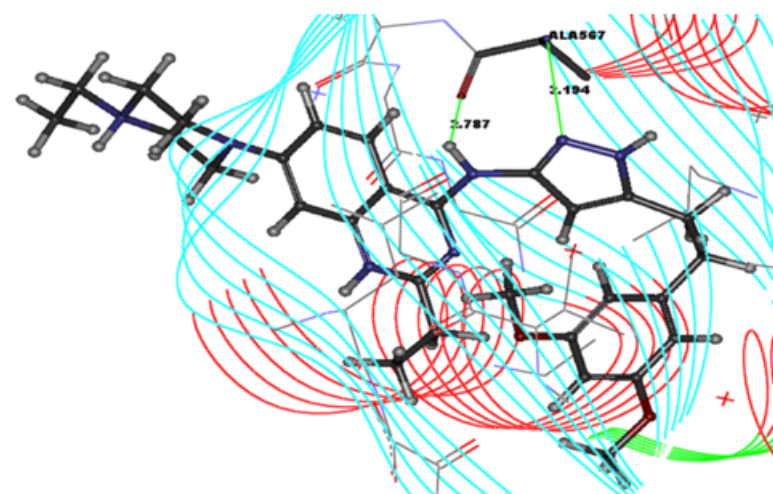


Fig. 7. The interactions of compound 5 with binding site residues of FGFR-2 according to rigid docking (for clarity certain aminoacids have been deleted)

FGFR2 with 4-aryl-2-phenylamino pyrimidine (PDBID: 1OEC) [34] and (6S)-6-phenyl-5,6-dihydrobenzo[h]quinazolin-2-amine (PDBID: 3R11) [35] which form two hydrogen bonds with Ala567. Based on pharmacophore hypotheses, 3D atom-based QSAR and docking, pyrazolylaminoquinazoline inhibitors can interact similarly to the ligands in co-crystals of FGFR2 PDBID: 1OEC [34] and 3R11 [35] which hamper the activation of the autoinhibited conformation of FGFR2 kinase. The ligands co-crystallized with FGFR2 in 1OEC and 3R11 co-crystals show significant inhibitory activity in cancer cells [35]. Since the inhibition of inactive kinases is an actual subject, the current investigation might provide a clue for the design of inhibitors that target the inactive conformations FGFR2 kinase.

## Conclusions

In the current investigation, we used pharmacophore modeling, 3D atom-based QSAR and docking to investigate pyrazolylaminoquinazoline potent FGFR2 inhibitors. The computational approach was thought-out to provide insight into the structural features of pyrazolylaminoquinazoline derivatives which determine their biological activity against FGFR2. The selected pharmacophore hypotheses are in accord with experimental interactions observed in FGFR2 co-crystals with ligands (1OEC and 3R11), whereas their afferent atom-based 3D-QSAR models displayed good correlative and predictive abilities ( $R$ -squared > 0.9,  $Q$ squared > 0.6,  $R$ -Pearson > 0.8). Binding orientations and interaction features of these molecules with FGFR2 were also investigated by docking experiments. Indeed, the

investigated compounds made contacts with critical residue Ala567, which was observed also in 1OEC and 3RI1 co-crystals, showing a good agreement between docking results and experimental data. Our results can and can guide the design of novel pyrazolyl-aminoquinazoline analogs with improved properties.

*Acknowledgements: The authors thank OpenEye Ltd. and Accelrys Software Inc. (for the Discovery Studio Visualiser v.2.5 program) for providing academic license and to Dr. Ramona Curpân (Institute of Chemistry Timisoara of Romanian Academy), for providing access to Schrödinger software acquired through the PN-II-RU-TE-2014-4-422 projects funded by CNCS-UEFISCDI Romania. This project was financially supported by Project 1.2 of the Institute of Chemistry of the Romanian Academy.*

## References

1. ESWARAKUMAR, V.P., LAX, I., SCHLESSINGER, J., Cytokine Growth Factor Rev., **16**, 2005, p. 139
2. PATEL, V.N., REBUSTINI, I.T., HOFFMAN, M.P., Differentiation, **74**, 2006, p. 349
3. GUO, M., LIU, W., SERRA, S., ASA, S.L., EZZA, S., Cancer Res., **72**, 2012, p. 2017
4. XU, R., RUDD, T.R., HUGHES, A.J., SILIGARDI, G., FERNIG, D.G., YATES, E.A., FEBS Journal, **280**, 2013, p. 2260
5. BHADORIYA, K.S., SHARMA, M.C., SHARMA, S., JAIN, S.V., AVCHAR, M.H., Arab. J. Chem., **7**, 2014, p. 924
6. JAIN, S.V., BHADORIYA, K.S., BARI, S.B., SAHU, N.K., GHATE, M., Med. Chem. Res., **21**, 2012, p. 3465
7. JAIN, S.V., GHATE, M., BHADORIYA, K.S., BARI, S.B., CHAUDHARI, A., BORSE, J.S., Org. Med. Chem. Lett., **2**, 2012, p. 22
8. SHARMA, M.C., SHARMA, S., SHARMA, P., KUMAR, A., BHADORIYA, K.S., J. Taiwan Inst. Chem. Eng., **45**, 2014, p. 12
9. BHADORIYA, K.S., SHARMA, M.C., JAIN, S.V., J. Mol. Struct., **1081**, 2015, p. 466
10. AVRAM, S., AVRAM, S., DEHELEAN, C., Rev. Chim. (Bucharest), **67**, no.1, 2016, p. 119
11. JAIN, S.V., BHADORIYA, K.S., BARI, S.B., Med. Chem. Res., 2012, **21**, 1665-1676.
12. KELLER, P.A., BIRCH, C., LEACH, S.P., TYSSSEN, D., GRIFFITH, R., J. Mol. Graph. Model., **21**, 2003, p. 365
13. IVAN, D., CRISAN, L., PACUREANU, L., Rev. Chim. (Bucharest), **62**, no.8, 2011, p. 806
14. JUN, F., YANG, D., JINGWEI, S., XIA, P., CHEN, W., SUFEN, C., BIN, Z., JING, A., MEIYU, G., WENHU, D., Bioorg. Med. Chem. Lett., **26**, 2016, p. 2594
15. \*\*\* Symyx Draw version 3.3, <http://symyxdraw.software.informer.com/3.3/>, 2010.
16. DIXON, S.L., SMONDYREV, A.M., KNOLL, E.H., RAO, S.N., SHAW, D.E., FRIESNER, R.A., J. Comput. Aided. Mol. Des., **20**, 2006, p. 647
17. DIXON, S.L., SMONDYREV, A.M., RAO, S.N., Chem. Biol. Drug. Des., **67**, 2006, 370
18. \*\*\* Schrödinger Release 2016-1: Phase, Schrodinger, LLC, New York, NY, 2016.
- 19.\*\*\* Small-Molecule Drug Discovery Suite 2016-1, Schrodinger, LLC, New York, NY, 2016.
20. \*\*\* Schrödinger Release 2016-1:LigPrep, Schrodinger, LLC, New York, NY, 2016.
21. WATTS, K.S., DALAL, P., MURPHY, R.B., SHERMAN, W., FRIESNER, R.A., SHELLEY, J.C., J. Chem. Inf. Model., **50**, **2010**, p. 534
22. \*\*\* Schrödinger Release 2016-1:ConfGen, Schrodinger, LLC, New York, NY, 2016.
- 23.\*\*\* OpenEye Scientific Software; Omega version 2.5.1.4, Santa Fe NM 87508; <http://www.eyesopen.com>, 2013.
24. HAWKINS, P.C.D., SKILLMAN, A.G., WARREN, G.L., ELLINGSON, B.A., STAHL, M.T., J. Chem. Inf. Model., **50**, 2010, p. 572
25. HAWKINS, P.C.D., NICHOLLS, A.N., J. Chem. Inf. Model., **52**, 2012, p. 2919
26. PEROLA, E., CHARIFSON, P.S., J. Med. Chem., **47**, 2004, p. 2499
27. KRISTAM, R., GILLET, V.J., LEWIS, R.A., THORNER, D., J. Chem. Inf. Model., **45**, 2005, p. 461
28. \*\*\* <http://www.rcsb.org/pdb/explore/explore.do?structureId=1OEC>, accessed in November 2016
29. OpenEye Scientific Software; Fred Receptor module version 2.2.5, Santa Fe NM 87508; <http://www.eyesopen.com>, 2013.
30. \*\*\* OpenEye Scientific Software; OEDocking version 3.0.1, Santa Fe NM 87508; <http://www.eyesopen.com>, 2012.
31. McGANN, M., J. Chem. Inf. Model., **51**, 2011, p. 578
32. McGANN, M.R., ALMOND, H.R., NICHOLLS, A., GRANT, J.A., BROWN, F.K., Biopolymers, **68**, 2003, p. 76
33. \*\*\* Discovery Studio Visualizer-Accelrys version 2.5 San Diego, CA. <http://accelrys.com>, 2009.
34. T.A. CESKA, R. OWENS, C. DOYLE, P. HAMLYN, T. CRABBE, D. MOFFAT, J. DAVIS, R. MARTIN, M.J. PERRY, The Crystal Structure of the FGFR2 Tyrosine Kinase Domain in Complex with 4-aryl-2-phenylamino pyrimidine Angiogenesis Inhibitors, To be published.
35. EATHIRAJ, S., PALMA, R., HIRSCHI, M., VOLCKOVA, E., NAKUCI, E., CASTRO, J., CHEN, C.R., CHAN, T.C., FRANCE, D.S., ASHWELL, M.A., J.Biol.Chem., **286**, 2011, p. 20677

Manuscript received: 23.05.2018

